Contrib Mineral Petrol (2007) 154:1–14
DOI 10.1007/s00410-006-0176-2

ORIGINAL PAPER

Thermochemistry of monazite-(La) and dissakisite-(La): implications for monazite and allanite stability in metapelites

E. Janots · F. Brunet · B. Goffé · C. Poinssot · M. Burchard · L. Cemič

Received: 25 September 2006 / Accepted: 15 December 2006 / Published online: 26 January 2007

Abstract Thermochemical properties have been either measured or estimated for synthetic monazite, $LaPO_4$, and dissakisite, $CaLaMgAl_2(SiO_4)_3OH$, the Mg-equivalent of allanite. A dissakisite formation enthalpy of –6,976.5 ± 10.0 kJ mol^{-1} was derived from high-temperature drop-solution measurements in lead borate at 975 K. A third-law entropy value of 104.9 ± 1.6 J mol^{-1} K^{-1} was retrieved from low-temperature heat capacity (C_p) measured on synthetic $LaPO_4$ with an adiabatic calorimeter in the 30–300 K range. The C_p values of lanthanum phases were measured in the 143–723 K range by differential scanning calorimetry. In this study, $La(OH)_3$ appeared as suitable for drop solution in lead borate and represents an attractive alternative to La_2O_3. Pseudo-sections were calculated with the THERIAK-DOMINO software using the thermochemical data retrieved here for a simplified metapelitic composition (La = ∑REE + Y) and considering monazite and Fe-free epidotes along the dissakisite-clinozoïsite join, as the only REE-bearing minerals. Calculation shows a stability window for dissakisite-clinozoïsite epidotes (T between 250 and 550°C and P between 1 and 16 kbar), included in a wide monazite field. The P–T extension of this stability window depends on the bulk-rock Ca-content. Assuming that synthetic $LaPO_4$ and dissakisite-(La) are good analogues of natural monazite and allanite, these results are consistent with the REE-mineralogy sequence observed in metapelites, where (1) monazite is found to be stable below 250°C, (2) around 250–450°C, depending on the pressure, allanite forms at the expense of monazite and (3) towards amphibolite conditions, monazite reappears at the expense of allanite.

Keywords Monazite · Allanite · Calorimetry · Thermodynamic properties · Phase diagrams · U–Th–Pb geochronology · Lanthanum

Communicated by J. Hoefs.

Electronic supplementary material The online version of this article (doi:10.1007/s00410-006-0176-2) contains supplementary material, which is available to authorized users.

E. Janots · F. Brunet · B. Goffé
Laboratoire de Géologie, ENS-CNRS UMR8538,
24 rue Lhomond, 75005 Paris, France

C. Poinssot
DEN/DPC/SECR, CEA, Saclay, France

M. Burchard
Institut für Geologie, Mineralogie und Geophysik,
Ruhr-Universität Bochum, Bochum, Germany

L. Cemič
Institut für Geowissenschaften der Universität Kiel
Olshausenstraße 40, 24098 Kiel, Germany

E. Janots (✉)
Institute of geological sciences, University of Bern,
Baltzerstrasse 3, 30012 Bern, Switzerland
e-mail: ejanots@geo.unibe.ch

Introduction

Although it is an accessory mineral, monazite, the light rare earth element (LREE) phosphate ($LREEPO_4$), is one of the main hosts for lanthanides and actinides in sedimentary, magmatic and metamorphic rocks. Its ubiquity as well as its chemical durability and its apparent resistance to radiation-induced amorphization confer to monazite the qualities of a robust U–Th–Pb

chronometer (e.g. Spear and Pyle 2002). Amongst the thermodynamic properties of REE-phases available, those of monazite are now relatively well constrained. Solubility products data (log K) have been measured for La, Nd and Sm monazite end-members (Rai et al. 2003; Poitrasson et al. 2004; Cetiner et al. 2005). Monazite formation enthalpy has been measured by high-temperature drop-solution calorimetry (Ushakov et al. 2001, 2004). Entropies of monazite have been derived only recently for Ce and La and Gd compositions by Thiriet et al. (2004) and Thiriet et al. (2005), respectively. The heat capacities (C_p) at high temperature (from 298 K to 1,600 K) were retrieved by Tsagareishvili et al. (1972). However, there is a lack of thermochemical properties for REE-minerals, which are likely to share phase relationships with monazite in metamorphic rocks. Consequently, the stability relations between monazite and allanite, the REE-epidote, have been mostly inferred indirectly from in situ U–Pb and Th–Pb geochronology data and mineral assemblages evolution along metamorphic transects (e.g. Wing et al. 2003; Janots et al. 2006). In metapelitic rocks, monazite stability (and geochronology) has long been thought to be restricted to medium and high-grade metamorphism typically above the greenschist facies conditions where allanite is the dominant REE-mineral (see Spear and Pyle 2002, for a review). At lower grade (including diagenesis), monazite is mostly considered as unstable (e.g. Harrison et al. 2002) or as detrital when present. However, recent studies show that monazite could crystallize under subgreenschist and low-temperature blueschist conditions (Rasmussen et al. 2001; Janots et al. 2006, respectively) or even during diagenesis (Evans and Zalasiewicz 1996; Evans et al. 2002).

We propose here to address monazite and allanite stability in metapelites by measuring or estimating the thermochemical data required to model their phase relationships. We have collected calorimetric data on synthetic analogues of LREE-minerals: $LaPO_4$ and dissakisite, $CaLaMgAl_2(SiO_4)_3OH$, the Mg-equivalent of allanite, which is the main LREE-bearing silicate in metamorphic rocks. Dissakisite was chosen in preference to allanite, although less relevant to metapelites, to avoid the difficulty of controlling and characterizing iron oxidation states in synthetic epidotes. Formation enthalpy, third-law entropy and C_p function have been derived from high-temperature solution calorimetry, low-temperature adiabatic calorimetry and differential scanning calorimetry, respectively. Then the measured data have been used to calculate pseudo-sections with the THERIAK-DOMINO program (Decapitani and Brown 1987) for a metapelitic bulk-rock composition. For the convenience of the reader, all mineral formulae and abbreviations encountered in this study have been recapitulated in the Appendix.

Experimental

Sample synthesis and characterization

Dissakisite, $CaLaMgAl_2(SiO_4)_3OH$, has been synthesized from stoichiometric tetraethylorthosilicate-based gels calcinated, beforehand, at 1,073 K (ambient pressure). This starting material was then run in a piston-cylinder apparatus at 1,023 K and 2.3 GPa for 6 days. $La(OH)_3$ was synthesized hydrothermally from La_2O_3 (99.99%) and deionized water at 773 K and 140 MPa for 8 days and then stored in air. Synthetic monazite, $LaPO_4$, was prepared by J.M. Montel (LMTG, Toulouse, France) according to the following procedure: in a first stage, a precipitate is obtained by adding phosphoric acid to a lanthanum nitrate solution. The precipitate, which, after drying was identified as rhabdophane-(La), $LaPO_4{\cdot}H_2O$, was baked at 1,525 K overnight, which then produces monazite. In a last stage, monazite crystals are grown in a Li_2MoO_4–MoO_3 flux for 1 week at 1,273 K; the flux is removed by dissolution in hot water. The monazite sample used for calorimetric measurements consists of homogeneous grains with sizes of about 50 μm.

All experimental products are single-phased as checked using X-ray diffraction data collected with a Siemens D5000 diffractometer at the Institute of Geosciences (Kiel University, Germany). In particular, the $La(OH)_3$ diffraction pattern did not show any detectable hydroxicarbonate or carbonate which can form in the course of the synthesis or during storage in air (Diakonov et al. 1998; Wood et al. 2002). Homogeneity, composition and grain size of the synthetic products were controlled using scanning electron microscopy (Hitachi S-2500 with EDS detector), Raman microspectroscopy (Renishaw spectrometer, λ = 532 nm, ENS-Paris, France) and electron microprobe analysis (SX-50, Jussieu, France). In addition, heat capacities measured with DSC have been compared to those derived from an oxide summation method (Berman and Brown 1985).

In order to achieve the reaction cycles required to retrieve formation-enthalpy data, additional sample powders were used for drop-solution measurements: α-Al_2O_3 (Merck, reagent grade) annealed at 1,300°C and stored under dry conditions, $CaCO_3$ (Aesar, 99.99%) and spinel $MgAl_2O_4$ (Kanto Chemicals, 99.9%). In addition, gem-quality specimens (mineral collection of the Ruhr-University, Bochum, Germany)

were used: Brazilian quartz (99.9% purity) and wollastonite, $Ca_{2.98–3.00}Si_{3.00–3.03}O_9$, from Kropfmuhl (Germany).

Calorimetric methods

Heat capacity (C_p) of synthetic monazite, $LaPO_4$, was measured between 30 and 300 K on 10.6 g of sample using the low-temperature adiabatic calorimeter described in Brunet et al. (2004). The calorimeter is equipped with two adiabatic shields and the sample temperature is measured with a platinum resistance thermometer. The powder sample is loaded under a He stream in a copper cell. Each experiment consists of a continuous temperature scan using 2 to 4 K steps and heating cycles of 300 to 600 s under a pressure of ~10^{-7} mbar. Heat capacity of the sample is obtained after subtracting the copper-cell contribution (see Brunet et al. 2004 for the heat capacity of the empty cell). The accuracy of C_p measurement is estimated to ±0.8 J mol^{-1} K^{-1} based on measurements on a reference compound (α-Al_2O_3, Furukawa et al. 1956). This accuracy can be converted into an entropy uncertainty (σ) of around 1.5% (Brunet et al. 2004).

Heat capacities were measured in the 143–323 K and 341–923 K ranges with an automated Perkin-Elmer DSC 7 (Institute of Geosciences, Kiel University, Germany). Temperature calibration, purge gas and other technical details are found in Bosenick et al. (1996) and Bertoldi et al. (2001) for the measurements in the high-temperature and low-temperature regions, respectively. Measurements are performed on 20–55 mg of sample placed in a gold pan (6-mm diameter) and covered with a thin gold lid. The heat-capacity data are obtained by measuring alternatively, a blank (empty pan), a standard for calibration (pan loaded with corundum) and the sample of interest (pan with sample). Heat capacities were collected in step-scanning mode as described in Bosenick et al. (1996), with a heating rate of 10 K min^{-1}. The C_p-calibration factor is obtained from synthetic corundum measurements, using the C_p function by Ditmars and Douglas (1971). Correction for Au-pan weight differences is calculated using the gold C_p polynomial by Robie et al. (1979).

Formation enthalpies were derived from high-temperature drop-solution calorimetry (Navrotsky 1997) in the Tian–Calvet twin calorimeter described by Kahl and Maresch (2001) and located at the Institute for Geology, Mineralogy and Geophysics (Ruhr University, Bochum, Germany). Sample pellets of 5–8 mg are dropped from room temperature (290–293 K) into a lead-borate solvent ($2PbO{\cdot}B_2O_3$) held at the calorimeter temperature (975 K). Measurements are performed under dynamic conditions (Navrotsky et al. 1994), i.e. under an argon stream (flow rate of 1.5 cm^3 s^{-1}), since volatile-bearing phases are investigated (e.g. carbonates and hydroxides). Before each set of measurements (typically, five measurements on both calorimeter sides), platinum scraps (30 mg) are dropped into the solvent in order to determine the calorimeter calibration factor. This continuous calibration reduces measurement error caused by changes of the temperature and electronic environment. Since samples are equilibrated, before being dropped, at a temperature between 290 and 293 K instead of 298.15 K (reference temperature), measured drop-solution enthalpy (ΔH_{ds}) are corrected using the C_p function of the sample, either tabulated ($CaCO_3$, Al_2O_3, SiO_2, $MgAl_2O_4$ and $CaSiO_3$) in Robie and Hemingway (1995) or measured here by DSC (dissakisite, $La(OH)_3$ and monazite).

Results

Heat-capacity data

The molar heat capacity of the following lanthanum phases monazite, dissakisite and lanthanum hydroxide was measured by DSC; temperature range, sample weight and C_p functions (Berman and Brown 1985; Maier and Kelley 1932) are recapitulated in Table 1.

In addition, monazite molar heat capacity was measured from 30 to 300 K using adiabatic calorimetry (electronic supplementary data). A ninth-order polynomial equation was fitted to the C_p data from 30 to 300 K and extrapolated down to absolute temperature using a cubic temperature approximation ($C_p = \alpha T^3$). Integration of these $C_p(T)/T$ functions between 40 to 298.15 K, and 0 to 40 K, respectively, yields a third-law entropy ($S°_{298}$) of 104.9 (1.6) J mol^{-1} K^{-1} for $LaPO_4$. Recently, Thiriet et al. (2005) proposed a $LaPO_4$ entropy of 108.24 J mol^{-1} K^{-1} from adiabatic data collected in the 2–380 K range. This entropy value is consistent with ours according to the uncertainty range (1–3%) proposed by Thiriet et al. (2005) for their C_p measurements. Accordingly, we will consider the mean third-law entropy value of 106.6 J mol^{-1} K^{-1} for $LaPO_4$, hereafter. Combining adiabatic and DSC data, the C_p function of monazite could be determined in the 30–723 K range with around 150 K overlap between the two independent datasets acquired on the same sample. These C_p data are plotted as a function of temperature in Fig. 1 along with data from previous studies (i.e. Thiriet et al. 2005; Tsagareishvili et al. 1972).

Table 1 Summary of the DSC data for synthetic monazite-(La), dissakisite-(La) and $La(OH)_3$

Sample	Weight (mg)	T range (K)	N (T_{low})	N (T_{sup})	Heat capacity polynomial
Monazite-(La)	38.7	143–723	5	5	$198.08 - 1{,}645T^{-0.5} - 1.323 \times 10^5 T^{-2} + 1.9276 \times 10^7 T^{-3}$ [a] $102.96 + 0.053T - 14.322 \times 10^5 T^{-2}$ [b]
Dissakisite-(La)	43.96	143–623	4	4	$743.18 - 6{,}116T^{-0.5} - 41.841 \times 10^5 T^{-2} + 44.4052 \times 10^7 T^{-3}$ [a] $421.91 + 0.142T - 93.838 \times 10^5 T^{-2}$ [b]
$La(OH)_3$	51.48	143–323	4	0	$207.97–1{,}401T^{-0.5} - 15.417 \times 10^5 T^{-2} + 15.0260 \times 10^7 T^{-3}$ [a] $95.26 + 0.101T - 9.720 \times 10^5\ T^{-2}$ [b]

N number of DSC scans on (T_{low}) = (143–323 K) and (T_{sup}) = (341–923 K)

[a] Berman and Brown (1985)

[b] Maier and Kelley (1932)

Since low-temperature C_p data have only been measured for monazite, the entropy of dissakisite has been approximated with the oxide summation method proposed by Holland (1989). This summation method includes a molar volume correction (S–V) to the entropy and can predict entropy within a few percents when the coordination of the oxide components is taken into account. In order to derive the dissakisite entropy, (S–V) P_2O_5 is taken from Brunet et al. (2004) and the other (S–V) values are taken from Holland (1989) apart from (S–V) La_2O_3 which was not available in the literature. A mean (S–V) value for La_2O_3 of 86.5 has been extracted from $LaPO_4$ monazite (this study), La_2O_3 (Cordfunke and Konings 2001a), $La(OH)_3$ (Chirico and Westrum 1980), $LaAlO_3$ (Schnelle et al. 2001) and $La_2Si_2O_7$ (Bolech et al. 1996). This mean value of 86.5 (irrespective the La coordination) permits to re-calculate the entropy of the five La-bearing phases used for the extraction within 5% ($R^2 = 0.961$) as shown in Fig. 2. Taking a dissakisite molar volume of 137.8 $cm^3\ mol^{-1}$, the predicted entropy of dissakisite is found to be equal to 309.9 $J\ mol^{-1}\ K^{-1}$.

Heat-capacity data for dissakisite could not be measured above 623 K due to thermal decomposition (dehydration) in the vicinity of that temperature. For the same reason, $La(OH)_3$ heat capacity could be measured up to 323 K only. Mean C_p value averaged over three to five DSC temperature scans are listed with their two standard deviations of the mean in electronic supplementary data. The precision for low-temperature (143–323 K) and superambient (341–723 K) DSC data is estimated to around 2–7% and 1–3%, respectively (Figs. 1, 3a, b). The low-temperature heat-capacity data for $La(OH)_3$ are consistent (within ±3%) with previous adiabatic measurements (Chirico and Westrum 1980, Fig. 3a). For further thermochemical calculations, equations were fitted to

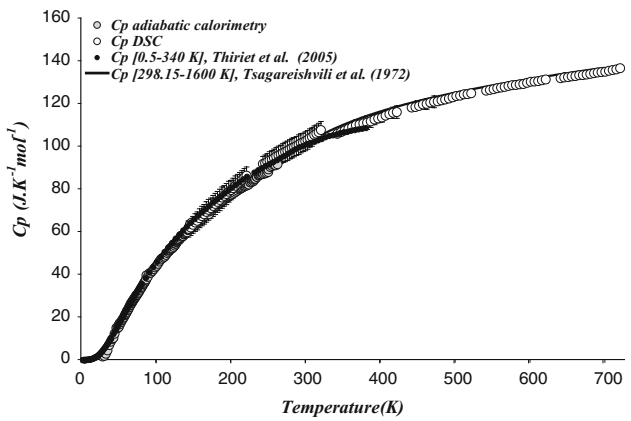

Fig. 1 $LaPO_4$ heat capacity measured using LT adiabatic calorimetry (30–300 K) and DSC (143–723 K). The C_p data from Thiriet et al. (2005) and Tsagareishvili et al. (1972) are also plotted for comparison

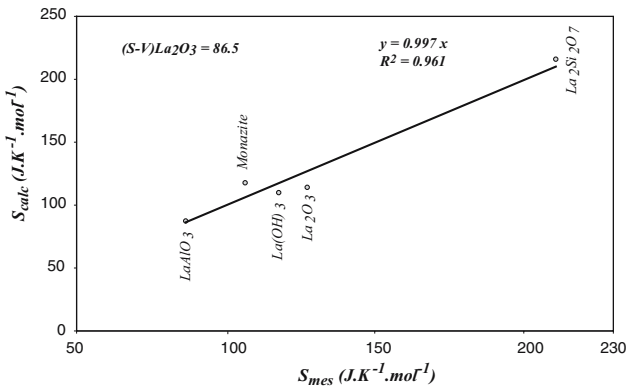

Fig. 2 Comparison between measured and calculated entropy values of $LaPO_4$ (this study), La_2O_3 (Robie et al. 1979), $La(OH)_3$ (Chirico and Westrum 1980), $LaAlO_3$ (Schnelle et al. 2001) and $La_2Si_2O_7$ (Bolech et al. 1996). Calculated value has been obtained by the oxide summation of Holland (1989) using a mean (S–V) La_2O_3 of 86.5 retrieved from these La-bearing phases

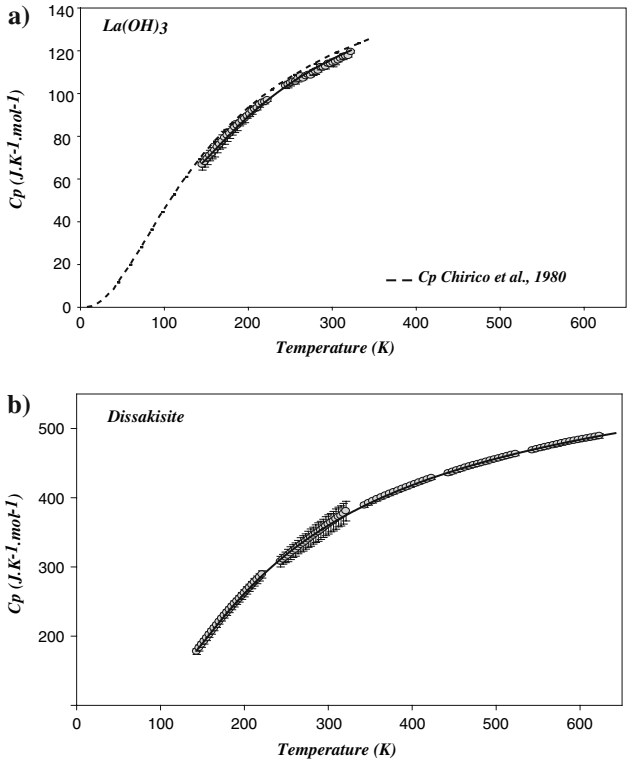

Fig. 3 Polynomial equation (*solid line*) of Berman and Brown's (1985) fitted to the DSC data obtained (*circles*) on **a** $La(OH)_3$ and **b** dissakisite-(La)

the heat-capacity data of all phases measured by differential scanning calorimetry using

1. the C_p polynomial proposed by Berman and Brown (1985) in order to be input in the database of Berman (1988):

$$C_p = k_0 + k_1 T^{-0.5} + k_2 T^{-2} + k_3 T^{-3}$$

(Table 1, Fig. 3).

2. the C_p polynomial proposed by Maier and Kelley (1932) in order to be added to the SUPCRT92 database (Johnson et al. 1992):

$$C_p = a + bT + cT^{-2}$$

(Table 1).

Formation-enthalpy data

Drop-solution enthalpies (ΔH_{ds}) for monazite and dissakisite and their reactant phases were measured in lead borate solvent at 975 K (Table 2). The reaction cycle used to derive dissakisite formation enthalpy $\Delta H°_{f,298}$ is given as an example in Table 3. Volatile components (H_2O and CO_2) are assumed to be totally released by the lead borate melt (Navrotsky et al. 1994) and flushed by the argon stream (i.e. under dynamic conditions). The dissolution enthalpy of $CaCO_3$ (Table 2) is consistent with published data obtained under similar dynamic conditions (Navrotsky et al. 1994; Kahl and Maresch 2001).

The $La(OH)_3$ formation enthalpy has been recalculated using our drop-solution value for $La(OH)_3$ (Table 2) combined to the drop-solution value for La_2O_3 (Bularzik et al. 1991; Robie et al. 1979) and La_2O_3 formation enthalpy (Cordfunke and Konings 2001a). We obtained a formation enthalpy of $La(OH)_3$ equal to –1,411.9 ± 4.6 kJ mol^{-1}, which compares well with the –1,416.1 ± 1.0 kJ mol^{-1} proposed by Diakonov et al. (1998). In addition, examination of lead borate solvent after dissolution reveals no evidence of undissolved particles or reaction products of $La(OH)_3$. Therefore, $La(OH)_3$ appears to be suitable for high-temperature dissolution experiments in lead borate solvent and, actually, it offers an interesting alternative to La_2O_3 which shows a sluggish dissolution rate and an exothermic enthalpy of solution in lead borate at 975 K (Helean and Navrotsky 2002).

The reaction cycle presented for dissakisite (Table 3) involves $CaCO_3$ and yields a formation enthalpy of –6,976.5 ± 10.0 kJ mol^{-1} (selected value for further thermochemical calculations, Table 4). A second cycle built up with $CaSiO_3$ instead of $CaCO_3$ yields $\Delta H°_{f,298}$ = –6,978.4 ± 9.9 kJ mol^{-1} for dissakisite. The good consistency between the formation enthalpy derived from these two reaction cycles validates the assumption of CO_2 degassing out of the solvent.

Monazite formation enthalpy was derived using the ΔH_{ds} value for P_2O_5 taken from Ushakov et al. (2001). Reaction cycle with $La(OH)_3$, considering white phosphorus as reference state, yields a value of –1,985.7 ± 3.0 kJ mol^{-1}, which compares well with the new dissolution data in $3Na_2O{\cdot}4MoO_3$ and in $2PbO{\cdot}B_2O_3$ solvents (–1,987.9 ± 2.0 kJ mol^{-1}) obtained by Ushakov et al. (2004).

Phase diagrams

The stability of monazite and dissakisite has been evaluated for a real metapelite composition expressed in the SiO_2–Al_2O_3–FeO–Fe_2O_3–MgO–CaO–Na_2O–K_2O–P_2O_5–La_2O_3–CO_2–H_2O system using the THERIAK-DOMINO software (Decapitani and Brown 1987). This software calculates equilibrium mineral assemblages for a specific bulk-rock composition (pseudo-sections). The thermochemical data derived in this study (Table 4) have been added to the updated database of Berman (1988), JUN92.bs, supplied with

Table 2 Corrected drop-solution enthalpies (ΔH_{ds}) obtained in this study along with literature data for comparison

Sample	ΔH_{ds} measured (kJ mol^{-1})	ΔH_{ds} literature (kJ mol^{-1})
Dissakisite, $CaLaMgAl_2(SiO_4)_3OH$	542.1 ± 7.3 (8)	
$La(OH)_3$	170.1 ± 3.8 (11)	
Monazite, $LaPO_4$	148.5 ± 2.2 (16)	154.6 ± 1.6 [a]
Calcite, $CaCO_3$	190.9 ± 0.8 (17)	191.1 ± 1.1 (7)[b]; 194.1 ± 0.9 [c]; 193.4 ± 0.7 (10)[d]; 189.6 ± 1.1 (9)[e]
Corundum, Al_2O_3	107.8 ± 1.9 (7)	107.4 ± 1.2 (22)[b]; 108.0 ± 1.0 [c]; 107.9 ± 1.0 (8)[d]
Quartz, SiO_2	38.8 ± 1.1 (8)	38.8 ± 0.8 (9)[b]; 38.4 ± 0.8 [c]; 39.1 ± 0.3 (9)[d]; 40.0 ± 0.2 (6)[f]
Spinel, $MgAl_2O_4$	164.8 ± 1.9 (7)	165.2 ± 1.0 [g]
Wollastonite, $CaSiO_3$	105.8 ± 3.1 (8)	105.4 ± 0.7 (8)[f]

Numbers in parentheses correspond to the number of measurements used to derive the drop-solution values

Reported uncertainties are two standard deviation of the mean

[a] Ushakov et al. (2004)

[b] Kahl and Maresch (2001)

[c] Grevel et al. (2001)

[d] Kisevela et al. (1996)

[e] Navrotsky et al. (1994)

[f] Chai and Navrotsky (1993)

[g] McHale et al. (1998)

Table 3 Thermochemical cycle used to derive the standard enthalpy of formation from the elements, $\Delta H_{f,el\ (298)}$, for dissakisite, $CaLaMgAl_2(SiO_4)_3OH$

Reaction		ΔH (kJ mol^{-1})
$CaLaMgAl_2(SiO_4)_3OH_{(298)} \rightarrow CaLaMgAl_2(SiO_4)_3OH_{(975)}$	(1) ΔH_{ds} $CaLaMgAl_2(SiO_4)_3OH$	542.1 ± 7.3
$CO_{2\ (298)} \rightarrow CO_{2\ (975)}$	(2) $\Delta H_{[298–975]}CO_2$	32.2
$CaCO_{3\ (298)} \rightarrow CaCO_{3\ (975)}$	(3) ΔH_{ds} $CaCO_3$	190.9 ± 0.8
$La(OH)_{3\ (298)} \rightarrow La(OH)_{3\ (975)}$	(4) ΔH_{ds} $La(OH)_3$	170.1 ± 3.8
$SiO_{2\ (298)} \rightarrow SiO_{2\ (975)}$	(5) ΔH_{ds} SiO_2	38.8 ± 1.1
$MgAl_2O_{4\ (298)} \rightarrow MgAl_2O_{4\ (975)}$	(6) ΔH_{ds} $MgAl_2O_4$	164.8 ± 1.9
$H_2O_{(298)} \rightarrow H_2O_{(975)}$	(7) $\Delta H_{[298–975]}H_2O$	25.1
$CaCO_3$+ $La(OH)_3$ + 3 SiO_2 + $MgAl_2O_4 \rightarrow CaLaMgAl_2(SiO_4)_3OH + CO_2 + H_2O$ $\Delta H(8) = -\Delta H(1) - \Delta H(2) - \Delta H(7) + \Delta H(3) + \Delta H(4) + 3\Delta H(5) + \Delta H(6)$	(8) $\Delta H^{\circ}_{ox,\ 298}$ $CaLaMgAl_2(SiO_4)_3OH$	42.9
$C_{(298)} + ½O_{2\ (298)} \rightarrow CO_{2\ (298)}$	(9) ΔH°_f CO_2[a]	–393.5 ± 0.1
$Ca_{(298)} + C_{(298)} + 3/2O_{2\ (298)} \rightarrow CaCO_{3\ (298)}$	(10) ΔH°_f $CaCO_3$[a]	–1,207.4 ± 1.3
$La_{(298)} + 3/2O_{2\ (298)} + 3/2\ H_{2\ (298)} \rightarrow La(OH)_{3\ (298)}$	(11) ΔH°_f $La(OH)_3$[b]	–1,416.1 ± 1.0
$Si_{(298)} + O_{2\ (298)} \rightarrow SiO_{2\ (298)}$	(12) ΔH°_f SiO_2[a]	–910.7 ± 1.0
$Mg_{(298)} + 2\ Al_{(298)} + 2\ O_{2\ (298)} \rightarrow MgAl_2O_{4\ (298)}$	(13) ΔH_f $MgAl_2O_4$[a]	–2,299.1 ± 2.0
$H_{2\ (298)} + ½O_{2\ (298)} \rightarrow H_2O_{(298)}$	(14) ΔH°_f H_2O[a]	–241.8 ± 0.0
$Ca + La_{(298)} + 3Si_{(298)} + Mg + 2\ Al + 0.5H_2 + 6.5O_2 \rightarrow CaLaMgAl_2(SiO_4)_3OH\Delta H(15) = \Delta H(8) - \Delta H(9) - \Delta H(14) + 2\Delta H(10) + \Delta H(11) + 3\Delta H(12) + \Delta H(13)$	(15) $\Delta H_{f,\ 298}$ $CaLaMgAl_2(SiO_4)_3OH$	–6976.5 ± 10.0

[a] Robie and Hemingway (1995)

[b] Diakonov et al. (1998)

the THERIAK-DOMINO software (http://www.titan.minpet.unibas.ch/minpet/theriak/theruser.html).

The consideration of P_2O_5, a main monazite constituent, led us to incorporate hydroxylapatite, $Ca_5(PO_4)_3OH$ (Robie and Hemingway 1995) to the database, as well. The solid solution between clinozoïsite and dissakisite was assumed to be ideal (REE in the A2 site, Rouse and Peacor 1993). Pseudo-sections have been calculated for a Ca-poor and Al-rich composition metapelite (Table 5, Fig. 4a) from the Central Alps, called MF131, described in Frey (1969). This sample is mainly constituted of quartz, chloritoid, white mica and chlorite assemblages which record sub-greenschist facies conditions (temperature around 350–400°C). In terms of REE-mineralogy, allanite ($Ca_{1.2}Fe_{0.8}Al_{2.2}(SiO_4)_3OH$) is found associated with chloritoid,

Table 4 Thermochemical data measured or estimated (bold) for monazite and dissakisite

Phase	$\Delta H_f°$ (kJ mol^{-1})	$S°$ (J K^{-1} mol^{-1})	$\Delta G_f°$ (kJ mol^{-1})	Heat-capacity polynomials
Monazite-(La)	–1,985.7 ± 3.0	106.6	–1,865.9	$198.08 - 1{,}645T^{-0.5} - 1.323 \times 10^5 T^{-2} + 1.9276 \times 10^7 T^{-3}$ [a] $102.96 + 0.053T - 14.322 \times 10^5 T^{-2}$ [b]
Dissakisite-(La)	–6,976.5 ± 10.0	**309.9**	–6,578.7	$743.18 - 6{,}116 \times T^{-0.5} - 41.841 \times 10^5 T^{-2} + 44.4052 \times 10^7 T^{-3}$ [a] $421.91 + 0.142T - 93.838 \times 10^5 T^{-2}$ [b]

[a] Berman and Brown (1985)

[b] Maier and Kelley (1932)

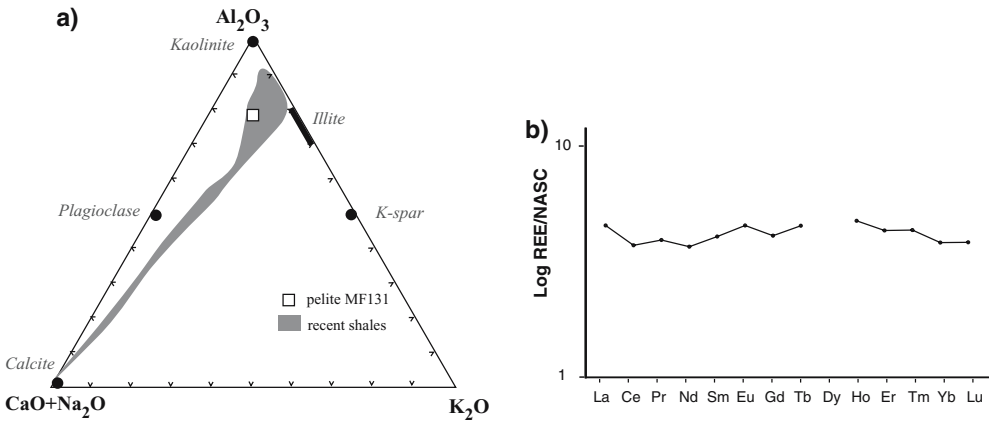

Fig. 4 **a** Bulk rock composition of the MF131 pelite plotted in an Al_2O_3–($CaO + Na_2O$)–K_2O ternary diagram with Common Cretaceous shales composition (Hutcheon et al. 1998); **b** NASC-normalized REE-pattern of the MF131 pelite (normalization data in Haskin et al. 1968)

whereas monazite is absent. Trace elements in MF131 were analysed by ICP mass spectrometry following a $LiBO_2$ fusion and nitric acid digestion of 0.2 g of sample (ACME lab, Canada). This metapelite is REE rich ($\sum$REE = 825 ppm) with a content of each REE around five times higher than that of the NASC reference (Haskin et al. 1968; Fig. 4b). For simplifications, lanthanum content was taken for the calculation as equal to the sum of REE and *Y*.

Table 5 Bulk rock composition (REE, oxides and elements) of an alpine metapelite (MF131) used as input for calculations with THERIAK-DOMINO software

REE	ppm	Oxide	wt.%	Element	mol%
Y	136.2	SiO_2	58.3	Si	19.01
La	146.8	TiO_2	0.84		
Ce	274.4	Al_2O_3	19.7	Al	7.57
Pr	31.3	Fe_2O_3	1.9	Fe_{tot}	2.32
Nd	122.3	FeO	6.8		
Sm	23.4	MnO	0.08	Mg	0.16
Eu	5.7	MgO	2.6	Ca	0.31
Gd	21.5	CaO	0.88	Na	0.46
Tb	3.9	Na_2O	0.73	K	1.08
Dy	24.8	K_2O	2.6	P	0.008
Ho	5.0	P_2O_5	0.06	La	0.006
Er	14.8	La_2O_3	0.01	C	0.35
Tm	2.2	CO_2	0.8	H	9.8
Yb	12.0	H_2O	4.6	O	58.50
Lu	2.0				
Sum	826.1	Sum	99.89		

The elemental composition (in mol%) has been normalized to 100% ignoring minor Ti and Mn

The pseudo-section obtained with the THERIAK-DOMINO program is represented in Fig. 5 for pressures and temperatures ranging from 1 to 16 kbar and 200 to 600°C, respectively. For MF131, the stability field of the clinozoïsite-dissakisite series (called REE-epidote hereafter) is found to be comprised between 250 and 550°C for pressures between 2 and 16 kbar. Monazite is basically stable in the rest of the *P*–*T* field displayed in Fig. 5. From 250°C (P = 2 kbar) to 450°C (P = 16 kbar), the monazite breakdown into REE-epidote (dissakisite component X_{Dsk} = 0.6 – 0.8) and apatite involves several silicates (reactions 1 to 9 in Fig. 5). In these reactions, the calcium is supplied by different minerals according to the *P*–*T* conditions: laumontite, lawsonite, wairakite (a low pressure phase) or omphacite. In most of the reactions (1 to 5; 6 and 7), dissakisite and apatite are associated with chloritoid. Above temperatures of 400–550°C, REE-epidotes (X_{Dsk} = 0.5 to 0.8) are no longer stable and monazite forms instead. Calcium is then taken up in anorthite and/or garnet, whereas

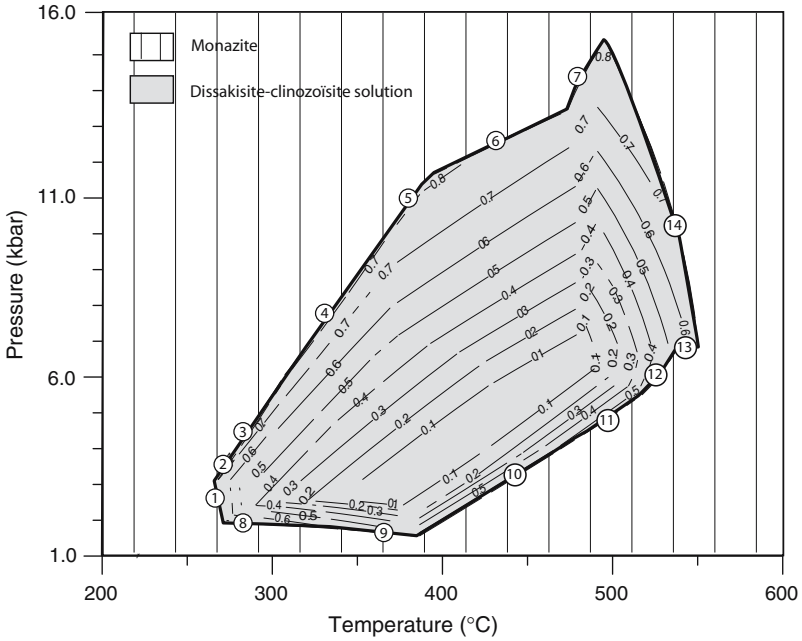

① KWM + Chl + Mnz + Lmt = KWM + Cld + Epd + Qtz + Hap + H_2O
② KWM + Chl + Lw Mnz + Cal = KWM + Cld + Epd + Hap + Qtz + H_2O + CO_2
③ Chl + Lw + Mnz = KWM + Cld + Epd + Hap + Qtz + H_2O
④ Bt + Lw + Mnz = KWM + Cld + Epd + Hap + Qtz + H_2O
⑤ Bt + Omp + Lw + Mnz = KWM + Cld + Epd + Hap + Qtz + H_2O
⑥ Bt + Omp + Lw + Cld + Mnz = Bt + KWM + Epd + Hap + Qtz + H_2O
⑦ KWM + Omp+ Lw + Mnz = Gt + Bt + KWM + Epd + Hap + Qtz + H_2O

⑧ Pl + Bt + Mnz + Wa = KWM + Cld + Epd + Hap + Qtz + H_2O
⑨ Bt + Mnz + Wa = KWM + Cld + Epd + Hap + Qtz + H_2O

⑩ KWM + Cld + Epd + Hap + Qtz = K-Fd + Pl + Bt + Mnz + H_2O
⑪ KWM + Cld + Epd + Hap + Qtz = Pl + K-Fd + Bt + Mnz + H_2O
⑫ Ab + Bt + KWM + Epd + Hap + Qtz = Gt + K-Fd + An + KWM + Cld + Mnz + H_2C
⑬ Gt + Bt + KWM + Epd + Hap + Qtz = Pl + K-Fd + KWM + Mnz + H_2O
⑭ Bt + KWM + Cld + Epd + Hap + Qtz = Gt + KWM + Mnz + H_2O

Fig. 5 THERIAK-DOMINO pseudo-section of the alpine metapelitic composition (MF131) highlighting the stability fields of monazite (*Mnz*) and dissakisite-clinozoïsite solution (*Epd*). Dissakisite-clinozoïsite isopleths are represented by the *lines with a number* corresponding to the dissakisite component (X_{Dsk}). The reactions between monazite and dissakisite (1 to 14) are summarized below the diagram with abbreviations described in the Appendix

magnesium and aluminum are mainly incorporated into mica (white mica or biotite). All the reactions from 1 to 14 correspond to water-producing reactions (with increasing temperature).

The respective stability of monazite and REE-epidote is expected to depend on the bulk composition of the hosting rock. In order to investigate the role of variable rock chemistry, additional calculations were performed using the THERIAK-DOMINO software on the MF131 composition with the concentration of a single element taken as variable. The influence of magnesium and iron variations cannot be reasonably considered as long as thermochemical data for allanite, $CaREEFeAl_2(SiO_4)_3OH$, are unknown. The effect of changing the bulk-rock calcium content between 0 and 5 mol% is displayed in Fig. 6. Whereas the temperature of the REE-epidote appearance (monazite breakdown) is unaffected, the breakdown temperature of REE-epidote increases with increasing calcium content (0 to 5 mol%): from 500 to 570°C at 5 kbar, from 570 to 810°C at 10 kbar and from 490 to more than 850°C at 15 kbar. This can be related to the epidote decomposition towards high temperatures, which involves the formation of garnet and plagioclase. For high Ca concentrations, the formation of these Ca-bearing alumino-silicates does not require the breakdown of REE-epidotes, abundant clinozoïsite acts as the calcium supply. Lanthanum and phosphorus concentrations will control the abundance of dissakisite, monazite and apatite but, unlike Ca concentration, they will have little effect on the temperature ranges of occurrences of these phases.

Discussion

Evaluation of the thermochemical data derived

In order to evaluate the accuracy of the formation enthalpy of $LaPO_4$ obtained by dissolution in lead borate, the solubility product (log K) of $LaPO_4$ was

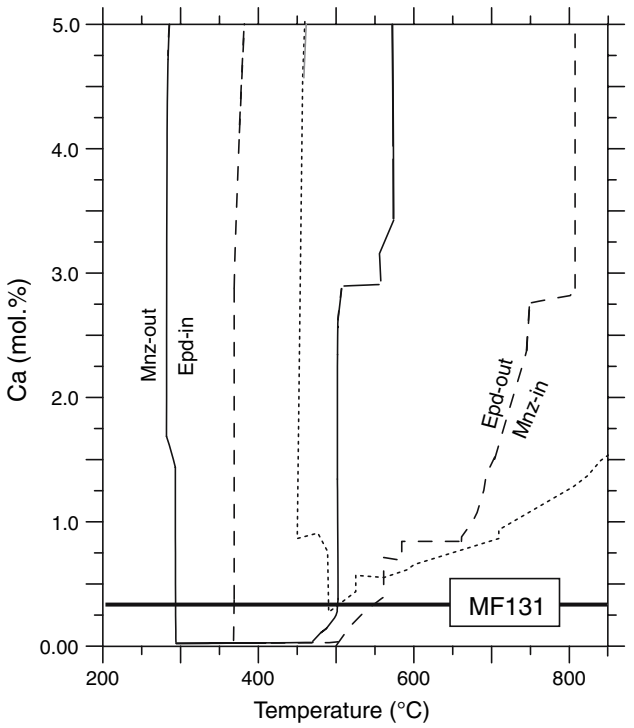

Fig. 6 Limits of monazite and Fe-free epidote stability fields as a function of temperature (at different pressures) and bulk-rock molar content of calcium. *Black solid*, *dashed* and *dotted lines* represent calculation at $P = 5$, 10 and 15 kbar respectively. *MF131* Ca-content is also plotted

calculated using the SUPCRT92 code (Johnson et al. 1992) and compared with literature data. In SUPCRT92, the thermochemical data for REE aqueous species are from Haas et al. (1995) and white phosphorus is used as reference state. The calculated solubility products have been determined using the following dissolution reaction:

$$LaPO_4 \rightarrow La^{3+} + PO_4^{3-}$$

While the experimental solubilities of hydrous La-phosphate are well documented (references in Poitrasson et al. 2004; Cetiner et al. 2005), those of monazite-(La) have only been determined by Cetiner et al. (2005) at 296.15 and 323.15 K, at atmospheric pressure. Figure 7 shows the calculated solubility products of $LaPO_4$ between 273.15 and 573.15 K at saturated vapour pressure compared to the experimental values of –24.7 ± 0.15 and –25.4 at 296.15 and 323.15 K, respectively (Cetiner et al. 2005). Calculations predict well the solubility decrease with temperature already documented by Poitrasson et al. (2004) and Cetiner et al. (2005). Even though, there is a general agreement between experimental solubility products measured on different monazite end-members, the calculated solubility products are three to four orders of magnitude lower than the experimental ones. The log K value of monazite-(La) compare well with those derived for Nd-, Sm- and Gd-composition, which are equal to –25.93 ± 0.07 and –25.8 ± 0.05 (Poitrasson et al. 2004; Cetiner et al. 2005, respectively), –24.55 ± 0.19 (Cetiner et al. 2005) and –25.84 (Poitrasson et al. 2004), respectively.

Assuming that the $LaPO_4$ third-law entropy is well constrained by low temperature adiabatic calorimetry, we can retrieve the formation enthalpy consistent with the experimental solubility data, as follows:

$$\Delta H^{\circ}_{f,T}(LaPO_4) = 2.306\,RT\log K + T\Delta S^{\circ}_{\mathrm{d,T}}(LaPO_4) + \Delta H^{\circ}_{f,T}(La^{3+}) + \Delta H^{\circ}_{f,T}(PO_4^{3-})$$

where

$$\Delta S^{\circ}_{d,T}(LaPO_4) = \Delta S^{\circ}_{f,T}(LaPO_4) - \Delta S^{\circ}_{f,T}(La^{3+}) - \Delta S^{\circ}_{f,T}(PO_4^{3-})$$

Considering that $\Delta S^{\circ}_{f,T}$ ($LaPO_4$) = 106.9 kJ mol^{-1} K^{-1} as determined in this study and using the data of aqueous species from the database of SUPCRT92, the experimental solubility product at standard conditions (log K = –24.7) yields a formation enthalpy of –1,963.2 kJ mol^{-1}. This value differs by around 20 kJ from those obtained by high temperature drop solution. It is important to note that a relatively small difference in term of enthalpy (around 1% of the value) influences remarkably the solubility product (three to four orders of magnitude). It remains difficult to interpret this discrepancy, which exceeds the uncertainty range of drop-solution data or solubility experiments. The revaluation of the standard properties of the La^{3+} (Cordfunke and Konings 2001b) shows that the source of error related to the lanthanum aqueous species is limited. Inconsistency between data using different reference states for phosphorus (e.g. red or white) has been looked for. The data in SUPCRT92 use the database of Wagman et al. (1982) for aqueous phosphorus species, where reference state for phosphorus is consistently taken as white phosphorus. In a similar way, the P_2O_5 thermochemical data, implemented in the high-temperature dissolution cycle (Robie and Hemingway 1995), are obtained using white phosphorus as reference state. The consistency

between drop-solution data obtained using different reactants for lanthanum (La_2O_3 and $La(OH)_3$) as well as different solvents (lead borate and sodium molybdate) demonstrates that high-temperature calorimetry is suitable to derive the formation enthalpy of monazite. Assuming that the source of the discrepancy lies in the solubility products derived experimentally, then the precipitation of a secondary metastable phase during monazite dissolution in acidic solution appears as a conceivable candidate. Although such secondary products have never been observed (Poitrasson et al. 2004; Cetiner et al. 2005), their formation cannot be excluded since it would explain the similarities between the solubility products measured for monazite and rhabdophane and, eventually, the apparent incongruent dissolution of monazite in acidic solution (Poitrasson et al. 2004; Cetiner et al. 2005). It must however be noted that such secondary precipitate, if any, is likely to involve Ostwald step processes (metastable intermediate phases) since the experimental solubility products are higher than the calculated ones (Fig. 7).

Without additional data, we propose to consider the value obtained in this study (–1,985.7 kJ mol^{-1}), keeping in mind that it does not fully account for experimental solubility products. We have tested the effect of changing the monazite enthalpy value from –1,985.7 to –1,963.2 kJ mol^{-1} on the calculated pseudo-section for the MF131 composition. Phase relations between monazite and REE-epidotes remain unchanged. However, the stability window of REE-epidote is extended towards larger temperature and pressure intervals of (200–700°C) and (0–20 kbar), respectively. Furthermore, epidote compositions closer to dissakisite end-member are stabilized.

Stability of monazite and allanite in metapelites

In order to evaluate the relevance of the thermochemical data derived here and to gain understanding on monazite- and allanite-forming reactions in metapelites, phase diagrams derived for MF131 have been compared to natural occurrences in metapelites.

The increasing use of monazite as a U–Th–Pb chronometer has led to a large number of descriptions of REE-assemblages in metapelites in order to better constrain and relate monazite ages to its *P–T* conditions of formation (e.g. Spear and Pyle 2002 and references therein). For example, Giere and Sorensen (2004) proposed that during prograde metamorphism, REE-mineralogy follows the general sequence:

detrital or igneous monazite ⇒ metamorphic allanite ⇒ metamorphic monazite.

Under low-grade conditions, monazite is usually considered to be metastable (detrital or igneous origin) although rare occurrences of newly formed monazite grains have been reported under diagenetic and subgreenschist facies conditions (Evans and Zalasiewicz 1996; Rasmussen et al. 2001; Evans et al. 2002; Wing et al. 2003; Bollinger and Janots 2006). In metapelites, monazite is often found to disappear to form prograde allanite at temperatures around 400°C (Smith and Barreiro 1990; Wing et al. 2003) and, eventually, to reappear at around 450 to 525°C (Smith and Barreiro 1990; Kingsbury et al. 1993; Franz et al. 1996; Wing et al. 2003). Nevertheless, recent studies point out that the temperature at which allanite decomposes to form monazite can be variable from one occurrence to another. Whole-rock composition and particularly Ca-content (Foster and Parrish 2003; Wing et al. 2003) may control this breakdown temperature.

The pseudo-section (Fig. 5) derived from our thermochemical data in a simplified system (La = $\sum$REE + *Y*) using dissakisite instead of allanite shows that, on the low-temperature side (Fig. 5), monazite has indeed a stability field. Under sub-greenschist facies conditions, dissakisite is stable consistently with the occurrence of allanite in the MF131 sample. In agreement with the crystallization sequence proposed by Giere and Sorensen (2004), monazite breaks down above 250°C to produce a La-rich epidote (X_{Dsk} = 0.6 to 0.8), the lanthanum content of which decreases with increasing temperature. This is in good agreement with the prograde allanite zoning patterns in metapelites (Fig. 8), which are characterized by REE-rich cores and Ca-rich rims, i.e. with a high clinozoïsite content (e.g. Oberli et al. 2004; Janots et al. 2006).

The calculated breakdown reactions of monazite can be compared to those reported from the literature. The REE-epidote forming reactions calculated here (reactions 1–9, Fig. 5) involve white mica, chlorite or biotite as reactants and white mica, biotite or chloritoid as products as already reported from natural occurrences (Broska and Siman 1998; Wing et al. 2003). In metapelites and metagranites, the calcium source to form REE-epidote along with apatite has been proposed to be plagioclase and/or carbonates (Broska and Siman 1998; Wing et al. 2003). However, according to our calculations calcium is rather supplied by different Ca-bearing phases as laumontite, lawsonite, wairakite

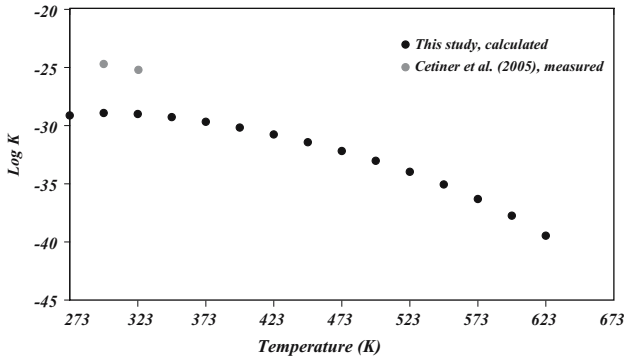

Fig. 7 Comparison of the experimental solubility product (Log *K*) of the monazite, $LaPO_4$, at 296.16 and 323.15 K (Cetiner et al. 2005) with those calculated with SUPCRT92 on the liquid vapour saturation curve

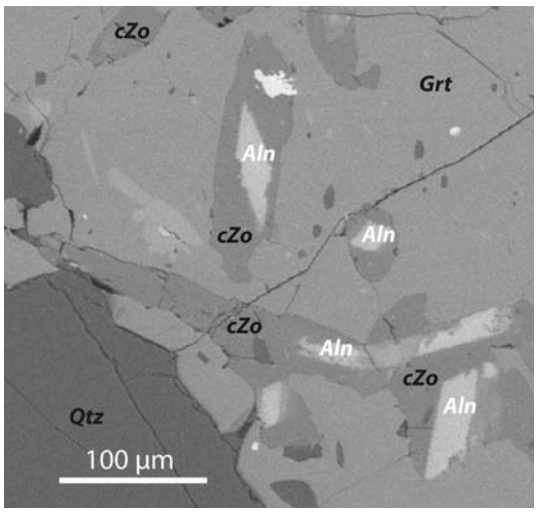

Fig. 8 Scanning electron microscope image showing epidotes with a REE-rich core (allanite *Aln*) and Ca-rich rim (clinozoïsite *cZo*) as inclusions in garnet (*Grt*) from a metapelite of Central Alps, MF307, described by Frey (1969)

or omphacite. This discrepancy may be explained by the preservation of detrital plagioclase in natural occurrences. This metastable plagioclase can then react, directly or not, to form allanite and apatite. With respect to carbonates, decarbonation to supply calcium is predicted only in reaction 2 around 280°C (Fig. 5)

There is a general agreement that along the allanite breakdown reactions, calcium is stored in plagioclase and garnet (e.g. Pyle and Spear 2003; Wing et al. 2003). This is consistent with all the prograde monazite-forming reactions calculated here (reactions 10–14, Fig. 5). The diagram in Fig. 6 shows that the increase of Ca concentration in the rock extends the allanite stability domain towards higher pressure and temperature. This is in good agreement with the REE-mineralogy in high-pressure rocks: while allanite is found in Ca-rich metabasite (e.g. Hermann 2002) monazite occurs in rocks with low CaO content (e.g. Krenn and Finger 2004 where CaO is below 0.8 wt.%).

Under retrograde metamorphic conditions, both REE-epidote and monazite can potentially form according to the phase diagram displayed in Fig. 5. Interestingly, the corresponding formation reactions are all water-consuming reactions. Therefore, the crystallization of retrograde monazite (or allanite) requires an aqueous fluid phase as already suggested from natural samples (Lanzirotti and Hanson 1996; Pan 1997; Broska and Siman 1998; Finger et al. 1998; Bollinger and Janots 2006).

In conclusion, we are aware that the generalization of the phase relations derived here to natural cases should be made with caution because (i) synthetic monazite-(La) and dissakisite-(La) are taken as analogues of natural monazite and allanite, (ii) the lack of consideration of other lanthanum or phosphate bearing-phases as florencite (Sawka et al. 1986; Rasmussen 1996; Nagy et al. 2002; Janots et al. 2006) or rhabodphane (Nagy et al. 2002), especially under low-grade conditions (iii) calorimetric data have been incorporated in an internally consistent database with optimized thermodynamic properties (Berman 1988). But despite these limitations, the phase relations in La-bearing systems derived in this study are broadly consistent with petrological observations and offer therefore new perspectives to interpret the occurrences of the two main REE-minerals in metamorphic rocks, monazite and allanite.

Acknowledgments This research project was financially supported by the NOMADE programme (CEA-CNRS) and by the SNF 20020–101826/1. We are grateful to J.-M. Montel who kindly provided us with synthetic $LaPO_4$ monazite. Assistance from J. Allaz and O. Schwarz (THERIAK-DOMINO software), N. Catel (wet chemical analyses), K.D. Grevel (HT drop-solution calorimetry), P. Kluge (DSC measurements), G. Marolleau (high-pressure devices) are gratefully acknowledged. We also thank C. Chopin and T. Parra for fruitful discussions. Constructive comments of S.V. Ushakov and an anonymous reviewer have significantly improved the quality of the manuscript and are appreciated.

Appendix

Table 6 Mineral formulae and abbreviations

Mineral	Structural formula	Abbreviation
Monazite	$LREEPO_4$	Mnz
Dissakisite	$CaREEMgAl_2(SiO_4)_3OH$	Dsk
Allanite	$CaREEFeAl_2(SiO_4)_3OH$	Aln
Dissakisite-clinozoïsite-(La) series	$Ca(Ca, La)(Mg, Al)Al_2(SiO_4)_3OH$	Epd
Florencite	$LREEAl_3(PO_4)_2(OH)_6$	
Rhabdophane	$LREEPO_4{\cdot}H_2O$	
Hydroxyapatite	$Ca_5(PO_4)_3OH$	Hap
Water	H_2O	
Quartz	SiO_2	Qtz
Clinozoïsite	$Ca_2Al_3(SiO_4)_3OH$	cZo
Laumontite	$CaAl_2Si_4O_{12}{\cdot}4(H_2O)$	Lmt
Lawsonite	$CaAl_2Si_2O_7(OH)_2{\cdot}H_2O$	Lw
Wairakite	$CaAl_2Si_4O_{12}{\cdot}2(H_2O)$	Wa
Calcite	$CaCO_3$	Cal
Omphacite solid solution	$(Ca, Na)(Al, Fe, Mg)Si_2O_6$	Omp
Plagioclase solid solution	$(Ca, Na)Al_{1\text{-}2}Si_{2\text{-}3}O_8$	Pl
Anorthite	$CaAl_2Si_2O_8$	An
Albite	$NaAlSi_3O_8$	Ab
Potassic feldspar	$KAlSi_3O_8$	K-Fd
Garnet solid solution	$(Ca, Mg, Fe, Mn)_3Si_3Al_2O_{12}$	Grt
Chorite solid solution	$(Al, Mg, Fe)_{3\text{-}4}(Al, Mg, Fe)_2(Si, Al)_4O_{10}(OH)_8$	Chl
Chloritoid solid solution	$(Fe,Mg)Al_2SiO_5(OH)_2$	Cld
Biotite solid solution	$K(Fe, Mg)_3(Si_3Al)O_{10}(OH)_2$	Bt
K White mica solid solution	$(K, Na)_{0\text{-}1}(Al, Mg, Fe)_{2\text{-}3}(Si,Al)_4O_{10}(OH)_2$	KWM

References

Berman RG (1988) Internally-consistent thermodynamic data for minerals in the system Na_2O–K_2O–CaO–MgO–FeO–Fe_2O_3–Al_2O_3–SiO_2–TiO_2–H_2O–CO_2. J Petrol 29:445–522

Berman RG, Brown TH (1985) Heat capacity of minerals in the system Na_2O–K_2O–CaO–MgO–FeO–Fe_2O_3–Al_2O_3–SiO_2–TiO_2–H_2O–CO_2: representation, estimation, and high temperature extrapolation. Contrib Mineral Petrol 89:168–183

Bertoldi C, Benisek A, Cemic L, Dachs E (2001) The heat capacity of two natural chlorite group minerals derived from differential scanning calorimetry. Phys Chem Mineral 28(5):332–336

Bolech M, Janssen F, Booij AS, Cordfunke EHP (1996) The standard molar enthalpies of formation of β-$La_2Si_2O_7$ and β-$Ce_2Si_2O_7$. J Chem Thermodyn 28(11):1319–1324

Bollinger L, Janots E (2006) Evidence for Mio-Pliocene retrograde monazites from the lesser Himalaya metamorphic series in Far Western Nepal. Eur J Mineral 18:289–297

Bosenick A, Geiger CA, Cemic L (1996) Heat capacity measurements of synthetic pyrope-grossular garnets between 320 and 1000 K by differential scanning calorimetry. Geochim Cosmochim Acta 60(17):3215–3227

Broska I, Siman P (1998) The breakdown of monazite in the West-Carpathian Veporic orthogneisses and tatric granites. Geol Carpath 49(3):161

Brunet F, Morineau D, Schmid-Beurmann P (2004) Heat capacity of lazulite, $MgAl_2(PO_4)_2(OH)_2$, from 35 to 298 K and a $(S - V)$ value for P_2O_5 to estimate phosphate entropy. Mineral Mag 68(1):123–134

Bularzik J, Navrotsky A, Dicarlo J, Bringley J, Scott B, Trail S (1991) Energetics of $La_{2-x}Sr_xCuO_{4-y}$ solid-solutions ($0.0 < x < 1.0$). J Solid State Chem 93(2):418–429

Cetiner ZS, Wood SA, Gammons CH (2005) The aqueous geochemistry of the rare earth elements. Part XIV. The solubility of rare earth element phosphates from 23 to 150°C. Chem Geol 217(1–2):147–169

Chai LA, Navrotsky A (1993) Thermochemistry of carbonate-pyroxene equilibria. Contrib Mineral Petrol 114(2):139–147

Chirico RD, Westrum EF (1980) Thermophysics of the lanthanide hydroxides. 1. Heat-capacities of $La(OH)_3$, $Gd(OH)_3$, and $Eu(OH)_3$ from near 5 K to 350 K lattice and schottky contributions. J Chem Thermodyn 12(1):71–85

Cordfunke EHP, Konings RJM (2001a) The enthalpies of formation of lanthanide compounds III. Ln_2O_3(cr). Thermochim Acta 375(1–2):65–79

Cordfunke EHP, Konings RJM (2001b) The enthalpies of formation of lanthanide compounds II. Ln^{3+} (aq). Thermochim Acta 375(1–2):51–64

Decapitani C, Brown TH (1987) The computation of chemical-equilibrium in complex-systems containing nonideal solutions. Geochim Cosmochim Acta 51(10):2639

Diakonov II, Tagirov BR, Ragnarsdottir KV (1998) Standard thermodynamic properties and heat capacity equations for rare earth element hydroxides. I. $La(OH)_3$(s) and $Nd(OH)_3$(s). Comparison of thermochemical and solubility data. Radiochim Acta 81(2):107–116

Ditmars DA, Douglas TB (1971) Measurement of relative enthalpy of pure α-Al_2O_3 (NBS heat capacity and enthalpy standard reference material no 720) from 273 to 1173 K. J Res Nat Bur Stand A Phys Chem 75(5):401–420

Evans J, Zalasiewicz J (1996) U–Pb, Pb–Pb and Sm–Nd dating of authigenic monazite: Implications for the diagenetic evolution of the Welsh Basin. Earth Planet Sci Lett 144(3–4):421–433

Evans JA, Zalasiewicz JA, Fletcher I, Rasmussen B, Pearce NJG (2002) Dating diagenetic monazite in mudrocks: constraining the oil window? J Geol Soc Lond 159:619–622

Finger F, Broska I, Roberts MP, Schermaier A (1998) Replacement of primary monazite by apatite-allanite-epidote coronas in an amphibolite facies granite gneiss from the eastern Alps. Am Mineral 83(3–4):248–258

Foster GL, Parrish RR (2003) Metamorphic monazite and the generation of P-T-t paths. In: Vance D, Müller W, Villa IM (eds) Geochronology: linking the isotopic record with petrology and textures, vol 220. Geological Society, London, Special Publications, pp 25–47

Franz G, Andrehs G, Rhede D (1996) Crystal chemistry of monazite and xenotime from Saxothuringian–Moldanubian metapelites, NE Bavaria, Germany. Eur J Mineral 8(5):1097–1118

Frey M (1969) Die Metamorphose des Keupers vom Tafeljuras bis zum Lukmanier-Gebiet, PhD thesis, Bern, p 160

Furukawa GT, Douglas TB, McCoskey RE, Ginnings DC (1956) Thermal properties of aluminum oxide from 0 K to 1200 K. J Res Nat Bur Stand 57(2):67–82

Giere R, Sorensen SS (2004) Allanite and other REE-rich epidote-group minerals. In: Epidotes, Rev Mineral Geochem 56, pp 431–493

Grevel KD, Schoenitz M, Skrok V, Navrotsky A, Schreyer W (2001) Thermodynamic data of lawsonite and zoisite in the system $CaO–Al_2O_3–SiO_2–H_2O$ based on experimental phase equilibria and calorimetric work. Contrib Mineral Petrol 142(3):298–308

Haas JR, Shock EL, Sassani DC (1995) Rare-earth elements in hydrothermal systems: estimates of standard partial molal thermodynamic properties of aqueous complexes of the rare-earth elements at high-pressures and temperatures. Geochim Cosmochim Acta 59(21):4329–4350

Harrison TM, Catlos EJ, Montel JM (2002) U–Th–Pb dating of phosphate minerals. In: Phosphates: Geochemical, geobiological, and materials importance. Rev Mineral Geochem 48, pp 523–558

Haskin LA, Haskin MA, Frey FA, Wildeman TR (1968) Relative and absolute terrestrial abundances of the rare earths. In: Ahrens LH (eds) Origin and distribution of the elements, Pergamon, New York, pp 889–911

Helean KB, Navrotsky A (2002) Oxide melt solution calorimetry of rare earth oxides - Techniques, problems, cross-checks, successes. J Therm Anal Calorim 69(3):751–771

Hermann J (2002) Allanite: thorium and light rare earth element carrier in subducted crust. Chem Geol 192(3–4):289

Holland TJB (1989) Dependence of entropy on volume for silicate and oxide minerals: A review and a predictive model. Am Mineral 74(1–2):5–13

Hutcheon I, Bloch J, De Caritat P, Shevalier M, Abercrombie H, Longstaffe F (1998) What is the cause of potassium enrichment in shales? In: Shales and mudstones; II, Petrography, petrophysics, geochemistry, and economic geology, E. Schweizervartsche Verlagsbuchhandlung, Stuttgart, pp 107–128

Janots E, Negro F, Brunet F, Goffe B, Engi M, Bouybaouene ML (2006) Evolution of the REE mineralogy in HP-LT metapelites of the Sebtide complex, Rif, Morocco: Monazite stability and geochronology. Lithos 87(3–4):214–234

Johnson JW, Oelkers EH, Helgeson HC (1992) Supcrt92—a software package for calculating the standard molal thermodynamic properties of minerals, gases, aqueous species, and reactions from 1 bar to 5000 bar and 0°C to 1000°C. Comput Geosci 18(7):899–947

Kahl WA, Maresch WV (2001) Enthalpies of formation of tremolite and talc by high-temperature solution calorimetry—a consistent picture. Am Mineral 86(11–12):1345–1357

Kingsbury JA, Miller CF, Wooden JL, Harrison TM (1993) Monazite paragenesis and U–Pb systematics in rocks of the eastern Mojave desert, California, USA—implications for thermochronometry. Chem Geol 110(1–3):147–167

Kiseleva I, Navrotsky A, Belitsky IA, Fursenko BA (1996) Thermochemistry and phase equilibria in calcium zeolites. Am Mineral 81(5–6):658–667

Krenn E, Finger F (2004) Metamorphic formation of Sr-apatite and Sr-bearing monazite in a high-pressure rock from the Bohemian Massif. Am Mineral 89(8–9):1323–1329

Lanzirotti A, Hanson GN (1996) Geochronology and geochemistry of multiple generations of monazite from the Wepawaug Schist, Connecticut, USA: implications for monazite stability in metamorphic rocks. Contrib Mineral Petrol 125(4):332–340

Maier CG, Kelley KK (1932) An equation for the representation of high temperature heat content data. J Am Chem Soc 54:3243–3246

McHale JM, Navrotsky A, Kirkpatrick RJ (1998) Nanocrystalline spinel from freeze-dried nitrates: synthesis, energetics of produce formation, and cation distribution. Chem Mater 10(4):1083

Nagy G, Draganits E, Demeny A, Panto G, Arkai P (2002) Genesis and transformations of monazite, florencite and rhabdophane during medium grade metamorphism: examples from the Sopron Hills, Eastern Alps. Chem Geol 191(1–3):25–46

Navrotsky A (1997) Progress and new directions in high temperature calorimetry revisited. Phys Chem Mineral 24(3):222–241

Navrotsky A, Rapp RP, Smelik E, Burnley P, Circone S, Chai L, Bose K (1994) The behaviour of H_2O and CO_2 in high-temperature lead borate solution calorimetry of volatile-bearing phases. Am Mineral 79(11–12):1099–1109

Oberli F, Meier M, Berger A, Rosenberg CL, Giere R (2004) U–Th–Pb and Th^{230}/U^{238} disequilibrium isotope systematics: precise accessory mineral chronology and melt evolution tracing in the Alpine Bergell intrusion. Geochim Cosmochim Acta 68(11):2543–2560

Pan Y (1997) Zircon- and monazite-forming metamorphic reactions at Manitouwadge, Ontario. Can Mineral 35:105–118

Poitrasson F, Oelkers E, Schott J, Montel JM (2004) Experimental determination of synthetic $NdPO_4$ monazite end-member solubility in water from 21°C to 300°C: Implications for rare earth element mobility in crustal fluids. Geochim Cosmochim Acta 68(10):2207–2221

Pyle JM, Spear FS (2003) Four generations of accessory-phase growth in low-pressure migmatites from SW New Hampshire. Am Mineral 88(2–3):338–351

Rai D, Felmy AR, Yui M (2003) Thermodynamic model for the solubility of $NdPO_4$(c) in the aqueous $Na^+–H^+–H_2PO_4^––HPO_4^{2–}–OH^––Cl^––H_2O$ system. J Radioanal Nucl Ch 256(1):37–43

Rasmussen B (1996) Early-diagenetic REE-phosphate minerals (florencite, gorceixite, crandallite, and xenotime) in marine sandstones: a major sink for oceanic phosphorus. Am J Sci 296(6):601–632

Rasmussen B, Fletcher IR, McNaughton NJ (2001) Dating low-grade metamorphic events by SHRIMP U–Pb analysis of monazite in shales. Geology 29(10):963–966

Robie RA, Hemingway BS (1995) Thermodynamic properties of minerals and related substances at 298.15 K and 1 bar (10^5 Pascals) pressure and at higher temperatures. In: U.S. Geological Survey Bulletin 2131, Government Printing Office, Washington, 461 p

Robie RA, Hemingway BS, Fisher JR (1979) Thermodynamic properties of minerals and related substances at 298.15 K and 1 bar (10^5 Pascals) pressure and at higher temperatures. In: U.S. Geological Survey Bulletin 1452, U.S. Government Printing Office, Washington, 454 p

Rouse RC, Peacor DR (1993) The crystal-structure of Dissakisite-(Ce), the Mg analogue of allanite-(Ce). Can Mineral 31:153–157

Sawka WN, Banfield JF, Chappell BW (1986) A weathering-related origin of widespread monazite in S-type granites. Geochim Cosmochim Acta 50(1):171–175

Schnelle W, Fischer R, Gmelin E (2001) Specific heat capacity and thermal conductivity of $NdGaO_3$ and $LaAlO_3$ single crystals at low temperatures. J Phys D Appl Phys 34(6):846–851

Smith HA, Barreiro B (1990) Monazite U–Pb dating of staurolite grade metamorphism in pelitic schists. Contrib Mineral Petrol 105(5):602–615

Spear FS, Pyle JM (2002) Apatite, monazite, and xenotime in metamorphic rocks. In: Phosphates: Geochemical, geobio-

logical, and materials importance, Rev Mineral Geochem 48, pp 293–335

Thiriet C, Konings RJM, Javorsky P, Wastin F (2004) The heat capacity of cerium orthophosphate $CePO_4$, the synthetic analogue of monazite. Phys Chem Mineral 31(6):347–352

Thiriet C, Konings RJM, Javorsky P, Magnani N, Wastin F (2005) The low temperature heat capacity of $LaPO_4$ and $GdPO_4$, the thermodynamic functions of the monazite-type $LnPO_4$ series. J Chem Thermodyn 37(2):131

Tsagareishvili DS, Gvelesia GG, Orlovskii VP, Belyaevskaya TK, Rep'ko VP (1972) Enthalpies and specific-heats of lanthanum, neodymium and yttrium orthophosphate at high temperature. Izv Akad Nauk SSSR Neorg Mater 8:1790–1793

Ushakov SV, Helean KB, Navrotsky A, Boatner LA (2001) Thermochemistry of rare-earth orthophosphates. J Mater Res 16(9):2623–2633

Ushakov SV, Navrotsky A, Farmer JM, Boatner LA (2004) Thermochemistry of the alkali rare-earth double phosphates, $A_3RE(PO_4)_2$. J Mater Res 19(7):2165–2175

Wagman DD, Evans WH, Parker VB, Schumm RH, Halow I, Bailey SM, Churney KL, Nuttall RL (1982) The NBS tables of chemical and thermodynamic properties. J Phys Chem Ref Data 11(2):392p

Wing BA, Ferry JM, Harrison TM (2003) Prograde destruction and formation of monazite and allanite during contact and regional metamorphism of pelites: petrology and geochronology. Contrib Mineral Petrol 145(2):228–250

Wood SA, Palmer DA, Wesolowski DJ, Bénézeth P (2002) The aqueous geochemistry of the rare earth elements and yttrium. Part XI. The solubility of $Nd(OH)_3$ and hydrolysis of Nd^{3+} from 30 to 290°C at saturated water vapor pressure with in-situ pH_m measurement. In: Hellmann R and Wood SA (eds) Water–rock interactions, ore deposits, and environmental geochemistry: a tribute to David A. Crerar, Geochemical Society Special Publication, vol 7, pp 229–256